ELSEVIER

Journal of Fluids and Structures 19 (2004) 669–680

JOURNAL OF FLUIDS AND STRUCTURES

www.elsevier.nl/locate/jnlabr/yjfls

Vortex-induced vibration of a heavy-lift launch vehicle during transonic flight

K.W. Dotson*, W.A. Engblom

The Aerospace Corporation, Mail Stop: M4/911, 2350 E. El Segundo Blvd., El Segundo, CA 90245-4691, USA

Received 16 September 2003; accepted 3 April 2004

Abstract

The Titan IV, like many other heavy-lift launch vehicles, is composed of three bodies. At Mach 1.1, 17-Hz pressure oscillations have been observed on the Titan IV center body. The associated lateral structural responses often exceed in amplitude those for all other flight events. Computational fluid dynamic (CFD) simulations conducted for the Titan IV show that pairs of vortices are shed due to strong crossflow acceleration towards the center body, and that these vortex pairs form periodically on alternate sides of the launch vehicle. The phenomenon is analogous to von Kármán vortex shedding over a cylinder, with Strouhal number 0.14–0.17. The CFD simulations were used to generate forcing functions for structural dynamic analyses. The resulting structural responses are in good agreement with transonic flight measurements. The structural dynamic analyses also show that the degree of alignment of the aerodynamic force amplitudes with the mission-specific structural mode shapes has a strong effect on the flight responses.
Published by Elsevier Ltd.

1. Introduction

Heavy-lift launch vehicles often consist of a core component flanked by two large (solid or liquid) rocket motors. The flanking motors are shorter than the core and have nose cones located aft of the payload fairing, which shrouds the spacecraft. The Titan IV launch vehicle has this general form and is shown in Fig. 1. Other three-body launch vehicles include the European Ariane 5, the Japanese H-II, the Russian Angara 3A, and the American Atlas V Heavy and Delta IV Heavy (Isakowitz et al., 1999).

1.1. Prediction of launch vehicle buffeting

The design of launch and space vehicles is established through analytical predictions of loads induced by flight events (Fleming, 1994; Kabe, 1998). However, only those flight events that establish the maximum response over a specified frequency band are analyzed. The maximum airloads event is generally critical and is composed of static aeroelastic, maneuvering, gust, and buffeting contributions (Kabe, 1998). Each of the maximum airloads components is defined by an independent loads analysis. A probability of nonexceedance is specified with each load result and with the total combined load (Kabe, 1998).

The buffeting contribution is generally maximized during transonic flight and is established using either transient- or frequency-domain analysis with dynamic models that correspond to a fixed flight time (Fleming, 1995). The buffeting

*Corresponding author. Tel.: +1-310-336-6629; fax: +1-310-336-8108.
E-mail address: kirk.w.dotson@aero.org (K.W. Dotson).

0889-9746/$ - see front matter Published by Elsevier Ltd.
doi:10.1016/j.jfluidstructs.2004.04.009

Fig. 1. Titan IV launch vehicle at liftoff. (Photo courtesy of Kennedy Space Center).

forcing functions are established from wind tunnel test data (Fleming, 1995; Cole et al., 2000) in which fluctuating pressures on a vehicle model are recorded for fixed combinations of Mach number, angle of attack, and side slip.

The launch vehicle model is generally rigid during the wind tunnel tests, but attempts have been made to quantify dynamic stability through the simulation of bending modes (Cole and Henning, 1991; Oswald et al., 1999). Semi-empirical methods (Dotson et al., 2000) and CFD (Oswald et al., 1999; Chen and Dotson, 2000) have also been used to assess launch vehicle aeroelasticity during transonic flight.

1.2. Titan IV flight experience

Forcing functions used in transient load analyses of the Titan IV buffeting environment were derived from wind tunnel test data (Black, 1988). However, since the inaugural flight in June 1989 there have been several updates to the Titan IV structural dynamic models and forcing functions to ensure that predicted launch vehicle and spacecraft loads are adequately conservative. These updates were generally introduced when post-flight data analyses revealed that the pre-flight analytical predictions were too low within some band of the analysis frequency range (0–50 Hz).

Post-flight data analysis for a recent Titan IV mission indicated a 17-Hz structural response level not seen on previous Titan IV missions, nor predicted in pre-flight buffet load analyses. The 0.8-g peak-to-peak pitch acceleration shown in Fig. 2 was measured on the core at vehicle station (VS) 169, that is, just aft of the payload fairing boattail; see Fig. 3. As indicated in Fig. 4, the maximum structural response occurred between free-stream Mach number 1.05 and 1.1 for this mission.

Fig. 5 shows response spectra, based on accelerations measured in the pitch direction at VS 169, for recurring flights of this configuration. Although all of these missions exhibited the 17-Hz structural response, the magnitude varied significantly. This flight-to-flight variability is attributed to sensitivity of the aerodynamic loading to angle of attack and side slip.

Flight instrumentation is intended for health monitoring and for the validation of analytical predictions. These data include an adequate mapping of flight accelerations but generally only limited measurements of flight pressure fluctuations. However, pressure measurements are made for the purpose of anomaly resolution or when they can be accommodated in the instrumentation suite. For the Titan IV launch vehicle, these occasional pressure measurements have identified flow-state fluctuations on the payload fairing not observed during wind tunnel tests (Dotson et al., 1998a, b), and they have motivated updates to the Titan IV buffet forcing functions.

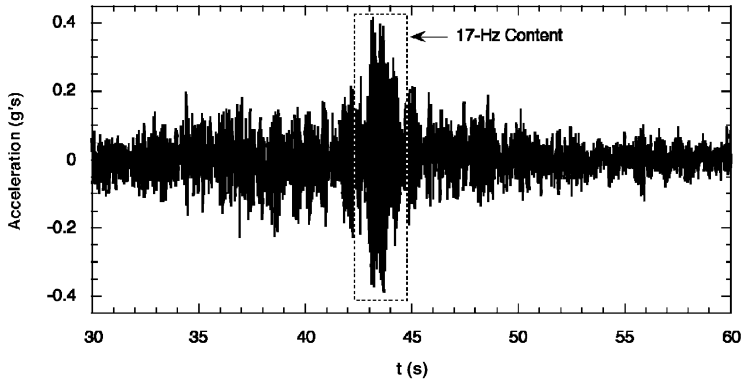

Fig. 2. Pitch acceleration on Titan IV core at VS 169 (0–50 Hz band-pass filtered).

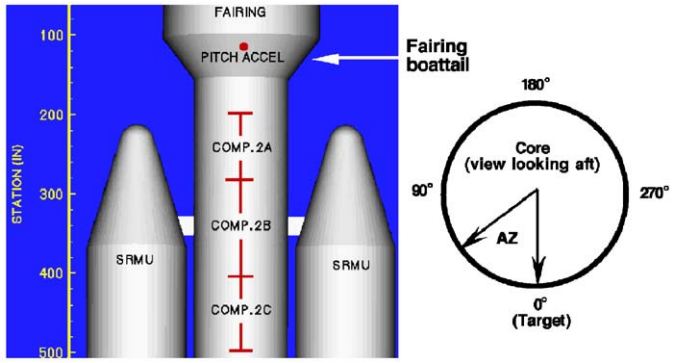

Fig. 3. Orientation of Titan IV vehicle stations and azimuths.

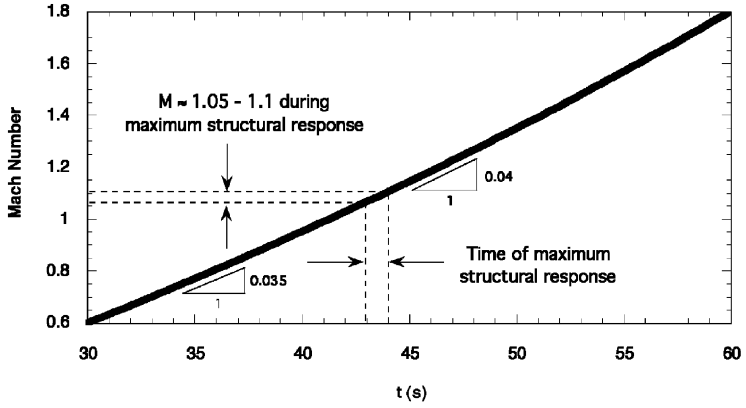

Fig. 4. Mach number for Titan IV mission.

2. Vortex shedding phenomenon

Fortunately, fluctuating pressure measurements were acquired on the core at several azimuths and at several vehicle stations for the Titan IV flight with the highest structural response, denoted by the heaviest line in Fig. 5. One of these time histories is shown in Fig. 6.

During the time of maximum structural response, 17-Hz pressure fluctuations were observed at several vehicle stations, with the maximum oscillations occurring between azimuths 30° and 60°. (See Fig. 3 for azimuth orientation.) Response spectra for pressure measurements near 60° azimuth and for three vehicle stations are shown in Fig. 7.

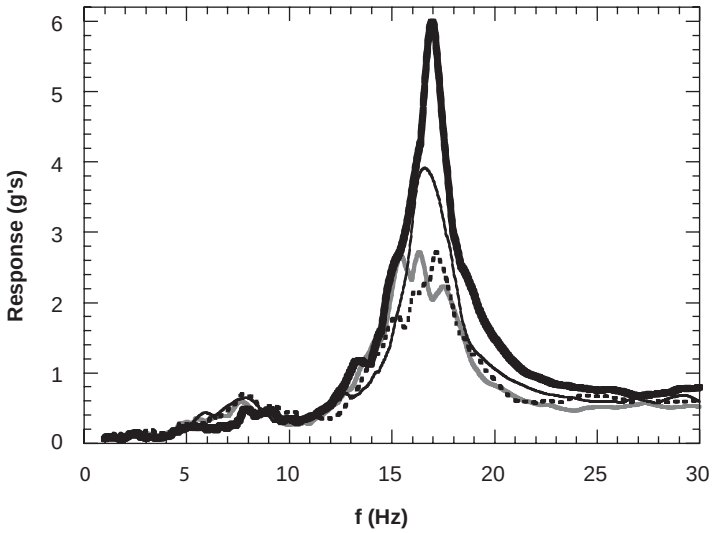

Fig. 5. Response spectra from 40–46 s time interval for pitch acceleration on Titan IV core at VS 169. Data set is composed of four recurring missions.

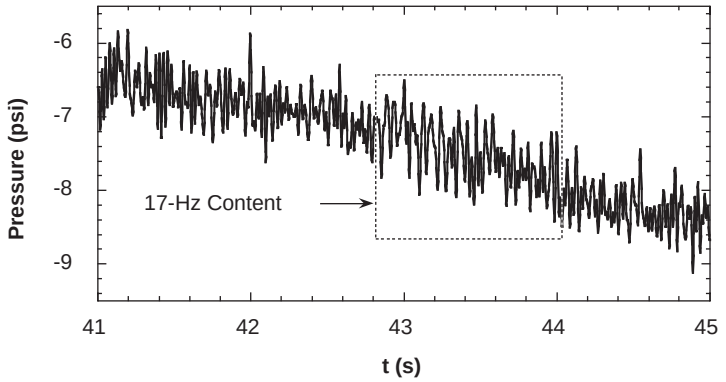

Fig. 6. Fluctuating pressure on Titan IV core at VS 270 and azimuth 65° (0–50 Hz band-pass filtered).

The discrepancy between pre-flight response predictions and flight accelerations was due to a deficiency in the Titan IV buffet forcing functions for frequencies around 17 Hz (Engblom, 2003). The forcing functions were updated based on these post-flight comparisons, and load predictions for all subsequent Titan IV missions have been adequately conservative.

An effort initiated to understand the transonic phenomenon included further flight data assessments, the reevaluation of Titan IV wind tunnel test data, and unsteady CFD analyses. During the latter, Engblom (2003) concluded that a mechanism exists which involves large vortex pairs that alternately shed from the core vehicle at a near constant primary frequency. This mechanism is shown schematically in Fig. 8.

The vortices form due to the crossflow acceleration of the annular flow that passes behind the hammerhead payload fairing. A portion of the flow is accelerated faster toward the core due to the presence of the solid rocket motor (SRMU) noses. This vortex-pair region is unstable and produces strong alternate vortex-pair shedding that can be captured analytically.

3. CFD Simulations

The CFD computations conducted in support of the post-flight assessment were documented by Engblom (2003). A summary of the analysis and results is provided in this section.

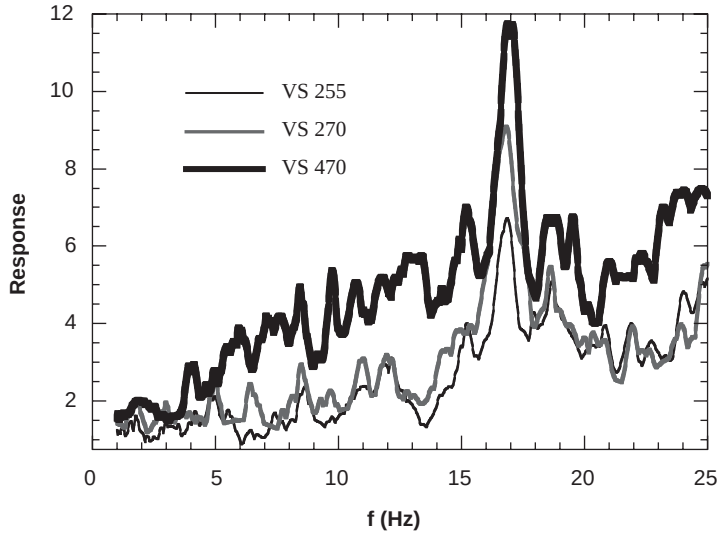

Fig. 7. Response spectra from 42–44 s time interval for pressure measurements at azimuth 60–65°.

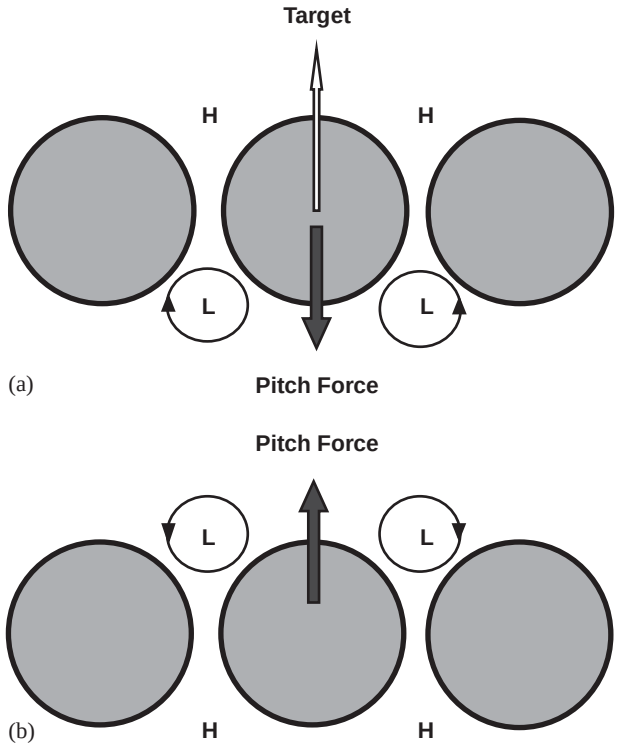

Fig. 8. Schematic of alternate vortex-pair shedding mechanism: (a) shedding opposite of target causes negative pitch force; (b) shedding on target side causes positive pitch force.

3.1. Background

The full 3-D, unsteady Navier–Stokes equations were integrated in a time-accurate manner. No symmetry planes were used. Both thin-layer and cross-derivative laminar viscous terms were included, but turbulence was omitted. The grid was exceptionally well resolved in the inviscid region along the core. The objective of the analysis was to capture

low-frequency transonic flow features that are evident in the flight data. These data indicate that the energy in the buffet environment hot spots is concentrated below 50 Hz.

A 3-D Titan IV surface geometry was developed, and a solid body model was constructed using I-DEAS, a computer-aided-design software (Structural Dynamics Research Corp., 1998). To reduce computational time, the portion of the Titan IV vehicle aft of VS 965 was not included in the CFD domain. Based on flight data, the primary buffeting behavior is expected to occur along the core, between the fairing boattail and the forward third of the flanking solid rocket motors. It is believed that reflections from the downstream boundary do not significantly influence the upstream flowfield because the free-stream is either near or above sonic speed in the CFD simulations.

The oscillatory displacements that correspond to the acceleration history in Fig. 2 have an amplitude of less than 0.03 in. (peak-to-peak). This maximum pitch displacement is extremely small relative to the diameters of the core and SRMU, which suggests that coupling between the vehicle motion and unsteady flowfield is negligible. The phenomenon, therefore, is not believed to be aeroelastic in nature, and the vehicle structure was assumed to be rigid in the simulations.

A grid containing approximately 4 million cells was generated, and is discussed at length by Engblom (2003). Mach numbers 0.8 and 1.1 were simulated. The angle of attack and side slip for both cases were taken to equal zero.

The commercial CFD code General Aerodynamic Simulation Program (GASPv3) was chosen as the flow solver for this effort (Aerosoft Inc., 1996). GASPv3 is a finite-volume, multi-block, structured-mesh code. The implemented numerical scheme to solve the full Navier–Stokes equations is second-order accurate in space and time. An explicit, two-step, Runge–Kutta algorithm was chosen for time-accurate computation.

Each simulation started with a uniform flowfield equivalent to the free-stream conditions. After approximately half a second of simulated real time, the solutions developed strong, self-sustained oscillatory behavior along the core. Each simulation was conducted for approximately one full second of physical time.

The simulations were computationally intensive. The maximum allowable time-step was typically 10^{-5} s. Since approximately 1 s of real-time simulation was conducted, each simulation required 10^5 steps: roughly 2 months of computation using 16 processors on a shared-memory Origin 2000.

3.2. Results

A map of the relative strength of the predicted buffet environment along the Titan IV surface is illustrated in Fig. 9. Specifically, the contours represent the root-mean-squared (rms) pressure fluctuations during the last 0.24 s of the simulation. The time interval is approximately three cycles of the primary fluid dynamic feature, to be described below. The other half of the vehicle surface is almost identical to Fig. 9.

The lack of symmetry in the solution is attributed primarily to the limited sample interval (0.24 s). It was verified that the multi-block grid is completely symmetric in size and distribution. A longer computation time, consequently, is required to achieve completely symmetric results.

The primary hot spots in Fig. 9 are caused by the alternate vortex-pair shedding mechanism. The strong pairs of vortices are alternately shed along the core at a nearly constant frequency: approximately 14 Hz for Mach 0.8. This alternation is illustrated in Fig. 10 for a transverse slice at VS 310. The mechanism results in a relatively large, unsteady, pitch-directed aerodynamic load applied to the core of the Titan IV vehicle.

The mechanics of the alternate vortex-pair shedding mechanism are complex. Animations of the crossflow plane suggest that vorticity is not being produced because of boundary layer separation, but rather by an inviscid-type streamline curvature effect. More specifically, due to the presence of the two SRMU nose cones, the flow accelerates towards the core from both sides; that is, two strong crossflow currents are created. These two crossflow currents (a) bifurcate upon reaching the core, (b) travel around a quadrant of the core, (c) impinge each other, which (d) causes vortices to form. Note that if this vorticity were formed due to boundary layer separation, the vorticity in Fig. 10 would be in the opposite direction.

Animations of the transient flowfield along the pitch plane suggest a plausible explanation for the unsteadiness of the phenomenon. Upon formation, the vortices act as severe obstructions to the free-stream flow. The free-stream flow, subsequently, diverts its local angle of attack towards the opposite side of the core, where a new pair of vortices are formed. This process repeats itself periodically.

The vortex pairs also lift off of the core surface as they convect downstream. This effect is expected due to the proximity of the vorticity vectors in each vortex pair. It is believed that the addition of a turbulence model would not have a significant effect on this mechanism.

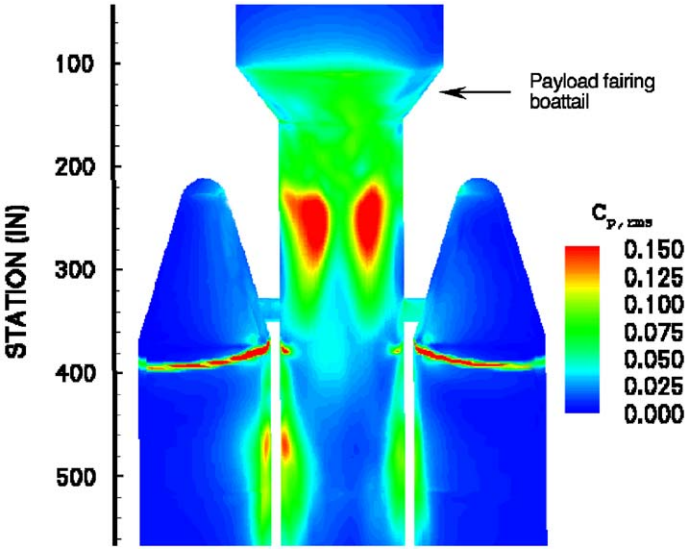

Fig. 9. Map of root-mean-squared fluctuating pressure at Mach 0.8.

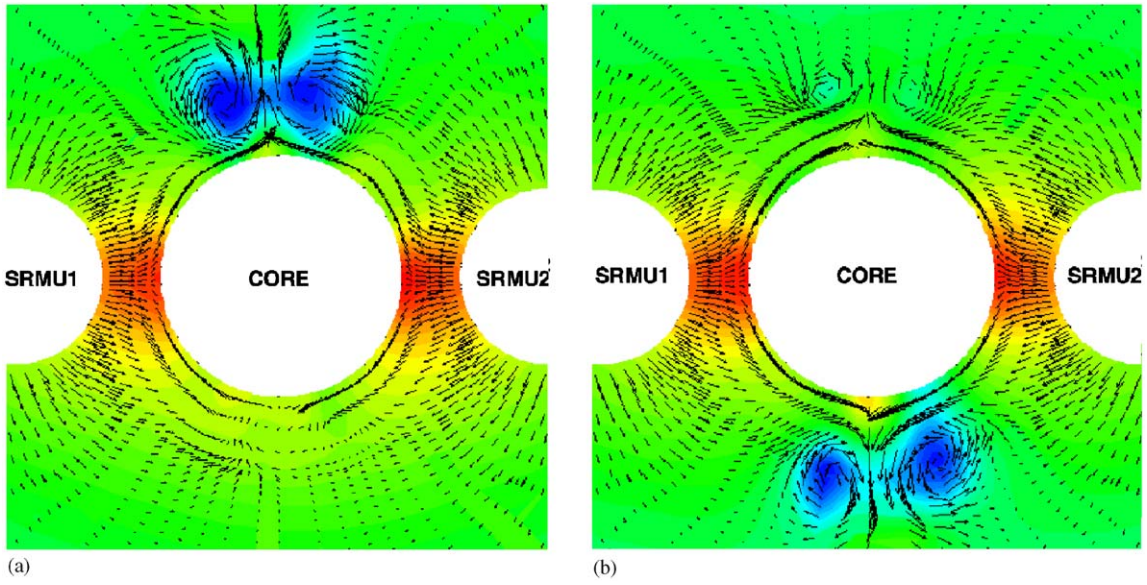

Fig. 10. Snapshots of pressure contours illustrating alternate vortex-pair shedding sequence at Mach 0.8: (a) pair of vortices (blue indicates low pressure region); (b) new pair of vortices on opposite side of core vehicle (0.035 s after snapshot in Fig. 10a).

4. Frequency content

The primary vortex-pair shedding frequency from the CFD simulations equaled approximately 14 and 21 Hz at Mach numbers 0.8 and 1.1, respectively (Engblom, 2003). Harmonics of this primary frequency were also observed. The primary mode of the vortex-pair shedding was dominant at Mach 0.8. The primary and secondary modes of the vortex-pair shedding were almost equally strong in the Mach 1.1 simulation.

Engblom (2003) also presented waterfall plots (of power spectral density for flight fluctuating pressures) that exhibit a variation in frequency with respect to time and, hence, Mach number. This frequency variation was compared with that from the simulations. The flight data and simulation results were in good agreement.

The observed increase in shedding frequency with free-stream Mach number (and velocity) is analogous to von Kármán vortex shedding over a cylinder. The frequency increase, moreover, suggests a near constant Strouhal (St) number of roughly 0.14 and 0.17 for the flight data and simulation results, respectively. The Strouhal number $St = fD/U_\infty$ was calculated based on the core diameter $D = 10$ ft and free-stream velocity $U_\infty = 850$ ft/s at Mach 0.8 and 1150 ft/s at Mach 1.1. Although this vortex-pair shedding mechanism is different from von Kármán vortex shedding, it is interesting to note that the Strouhal numbers 0.14 and 0.17 are relatively close to those for von Kármán vortex-shedding (Schlichting, 1979).

5. Structural dynamic analysis

A Mach 1.0 structural dynamic model was generated for the Titan IV missions with the flight response spectra shown in Fig. 5. A transient response analysis was then conducted using forcing functions developed from the CFD results. The objective of the analysis was to determine if the CFD simulations yield responses that are consistent with those observed in flight.

5.1. Forcing function development

The forcing functions for the transient analysis were derived from the CFD simulations for Mach 0.8 because, as mentioned in the previous section, the primary vortex-pair shedding mode was most evident in these results.

Recall that the angle of attack and side slip values equal zero in the CFD simulations. These conditions are nominal because launch vehicle trajectories are designed to minimize the static aeroelastic loads experienced during flight (Kabe, 1998; Dotson et al., 1998b).

The start-up transient in the CFD simulation was deleted, such that only the (roughly) periodic portion was retained for the construction of the buffet forcing functions. The remaining 0.24 s segment of the Mach 0.8 simulation was next added repeatedly end-to-end to generate a longer, synthetic time history. The spurious frequency content introduced by this concatenation was eliminated using high-pass filtering. The fluctuating pressures in the simulation were then integrated to yield 14 pitch forcing functions, corresponding to the grid points in the structural model between vehicle stations 113 and 500.

Recall that the primary frequency of the Mach 0.8 simulation results equaled approximately 14 Hz. The time step of the forcing functions was next manipulated to yield a synthetic frequency increase commensurate with flight experience. Although a wider range of vortex-pair shedding frequencies is apparently possible, the dynamic analysis was limited to roughly 16–18 Hz excitation so that the predicted responses could be reasonably compared with the flight response shown in Fig. 2.

The rate of change of the vortex-pair shedding frequency was defined by $\Delta f = \mathrm{St}(c\Delta M/D) = 0.54$ Hz/s, where the speed of sound c equals 1050 ft/s, $\mathrm{St} = 0.14$, $D = 10$ ft, and the Mach number rate of change $\Delta M = 0.037$/s (see Fig. 4). The analysis duration was taken conservatively to equal 4.25 s.

The first second for two of the 14 analysis forcing functions is shown in Fig. 11. Note that the pitch force for aft vehicle stations (Fig. 11(b)) includes frequency components associated with higher harmonics of the primary vortex-pair shedding frequency (Engblom, 2003).

5.2. Predicted structural response

A response spectrum corresponding to the predicted pitch acceleration at VS 169 is compared in Fig. 12 with the response spectrum for the largest observed flight response, that is, the heaviest line in Fig. 5. The spectra are in remarkably good agreement, but the peak of the analysis spectrum is somewhat higher than the corresponding flight value. This is expected because the prolonged periodicity of the analytical buffet forcing functions represents a limiting case. That is, angle of attack and side slip changes inherent to flight trajectories can be expected to perturb the vortex-pair shedding.

It was concluded, based on this structural dynamic analysis, that unsteady CFD can be used to conservatively predict structural responses from alternate vortex-pair shedding. These simulations are particularly useful if the wind tunnel tests lack adequate resolution to capture the phenomenon.

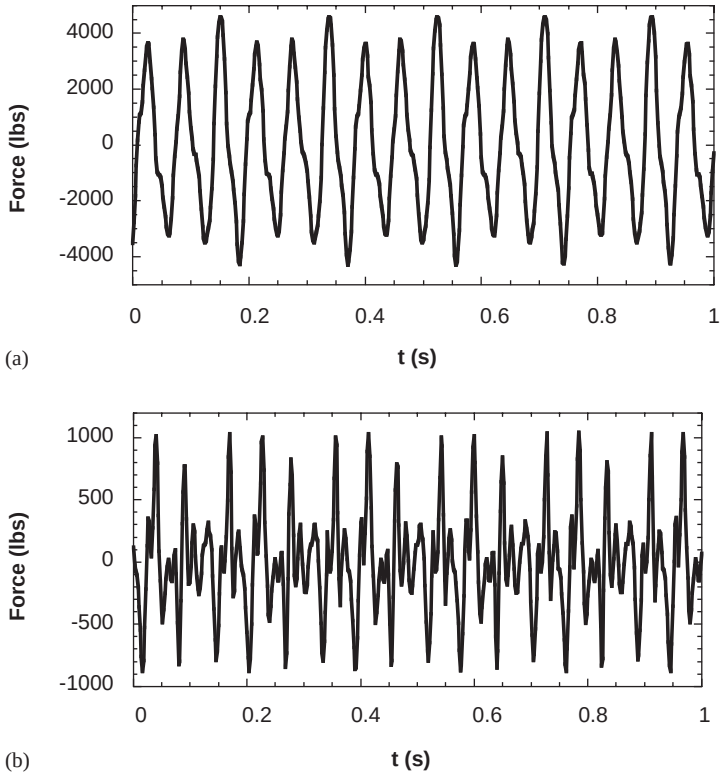

Fig. 11. First second of two forcing functions derived from CFD simulation at Mach 0.8: (a) vehicle station 283; (b) vehicle station 459.

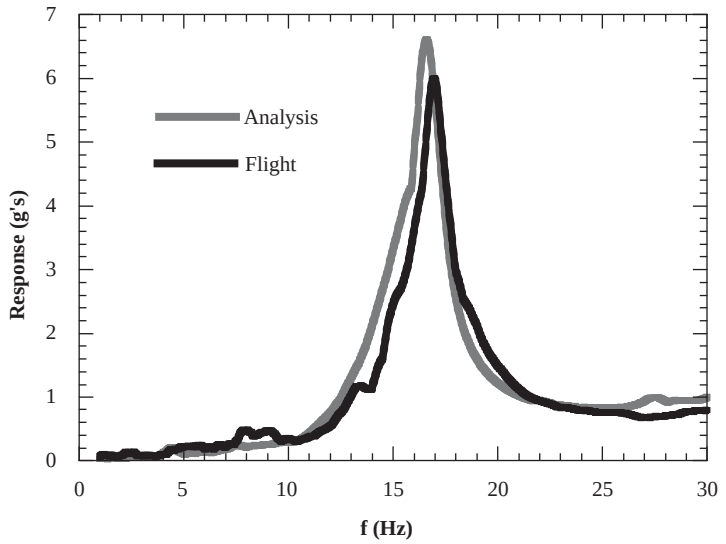

Fig. 12. Response spectra for pitch acceleration. Largest flight response vs. analytical response computed using CFD-derived forcing functions.

5.3. Importance of modal gain

In this section, the Titan IV missions with the response spectra shown in Fig. 5 are referred to as configuration A. A review of the coupled launch vehicle/space vehicle model for configuration A indicates that four pitch bending modes in the frequency range 16–18 Hz have significant gains, as well as phasing consistent with flight acceleration measurements.

The pitch degrees of freedom of the launch vehicle structure are illustrated in Fig. 13(a) for the four bending modes. Note that the shapes of these closely spaced modes are very similar. Differences in the mode shapes exist for spacecraft and upper stage degrees of freedom, which are not illustrated in Fig. 13(a).

The amplitude of the pitch aerodynamic force from the Mach 0.8 simulation is superimposed in Fig. 13(a). It is evident that the forces from alternate vortex-pair shedding are nearly ideal for excitation of all four of these pitch bending modes. In particular, the vehicle station of the maximum simulation force (VS 265) is very close to a local maximum for all four of the mode shapes (VS 283).

A similar review of modal data for other Titan IV missions (with different upper stages and spacecraft) revealed that the confluence of the bending mode shapes with the vortex-pair shedding force distribution does not exist across the Titan IV fleet. This explains why the observed flight structural responses are strongly dependent on the spacecraft and upper stage combination.

As an example, Fig. 13(b) shows pitch bending modes in the frequency range 16–18 Hz for Titan IV configuration B, which has a different upper stage and spacecraft than configuration A. Note that only two pitch bending modes exist in the frequency range of the observed vortex-pair shedding.

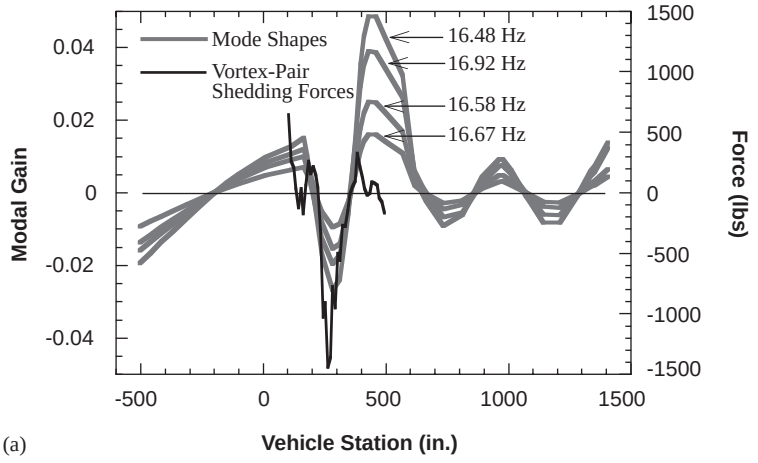

Fig. 13. Comparison of shapes for pitch modes in frequency range 16–18 Hz with pitch force amplitude from Mach 0.8 CFD simulation: (a) Titan IV configuration A; (b) Titan IV configuration B.

The shapes of these two modes, moreover, do not coincide ideally with the aerodynamic force amplitude, as do the mode shapes shown in Fig. 13(a). Note, in particular, that the payload fairing portion (vehicle stations <165 in.) of the two mode shapes for configuration B is generally out of phase with the vortex-pair shedding forces, but is in phase with respect to these forces for configuration A. The aerodynamic forces acting on the payload fairing, therefore, increase the generalized forces for configuration A, but decrease the generalized forces for configuration B.

It is evident from this modal comparison that the structural dynamic model should be carefully constructed and that the responses induced by alternate vortex-pair shedding for any given three-body launch vehicle are sensitive to changes in the upper stage or spacecraft.

5.4. Effects of linear sweep rate

Because wind tunnel tests are conducted at a fixed Mach number, forcing functions derived from wind tunnel data are stationary and do not account for the frequency increase with Mach number of the flight vortex-pair shedding. Consequently, wind tunnel-derived forcing functions may significantly overpredict structural responses when coupled system bending modes exist at the frequencies of vortex-pair shedding captured in wind tunnel tests.

For example, the pitch bending mode with the highest modal gain in Fig. 13(a) has natural frequency 16.5 Hz and 0.64% of critical damping. Recall that the linear sweep rate equals 0.54 Hz/s. Using data presented by Lollock (2002), it is easy to show that the swept linear forcing functions generate a maximum response that is approximately 60% of the value for steady-state excitation. In other words, buffet forcing functions derived from wind tunnel test data that exhibit 16.5 Hz steady-state vortex-pair shedding would overpredict the structural response for this bending mode by approximately $(1/0.60 - 1) \times 100 = 67\%$. This overprediction is quite significant and, of course, would be even larger if the structural damping value were lower, or if the time rate of increase in the Mach number were higher.

6. Conclusions

Bodies that flank the core of a launch vehicle obstruct the flow and can cause organized vortex shedding. The existence of this phenomenon for the Titan IV launch vehicle and its effect on flight structural responses raise concerns for three-body launch vehicle configurations in general. However, the geometry of the core and flanking bodies is expected to have an influence on the phenomenon, and the findings reported herein should not be regarded as strictly applicable for all launch vehicles in this class.

However, the study does emphasize that wind tunnel test programs and CFD analyses developed for three-body launch vehicles should pay particular attention to this phenomenon. It also indicates that CFD can be used for preflight predictions or to supplement wind tunnel data when the test instrumentation does not adequately resolve the alternate vortex-pair shedding.

Because of recent improvements in computational speed and grid generation, parametric studies of this unsteady phenomenon are becoming feasible. Additional work is needed to further investigate the effect of Mach number, angle of attack, and side slip on vortex-pair shedding. In particular, these parameters should be assessed to ensure that their effects on the buffet forcing functions are understood and that flight structural responses are conservatively predicted.

References

Aerosoft Inc., 1996. General Aerodynamic Simulation Program (GASP) User Manual Version 3, Blacksburg, VA, USA.

Black, J.A., 1988. A Wind Tunnel Investigation of the Buffet Characteristics of Truncated 0.079-Scale Models of the Titan III and Titan IV Launch Vehicles at Mach Numbers from 0.60 to 1.60. AEDC-TSR-88-P25, Arnold Engineering Development Center, Tullahoma, Tennessee, USA.

Chen, S.-H., Dotson, K.W., 2000. A time-marching aeroelastic analysis of launch vehicles in transonic flow. In: Proceedings of the International Forum on Aeroelasticity and Structural Dynamics, ATR-2000(8424)-1, The Aerospace Corporation, Los Angeles, CA, USA.

Cole, S.R., Henning, T.L., 1991. Dynamic response of a hammerhead launch vehicle wind-tunnel model. In: Proceedings of the 32nd AIAA/ASME/ASCE/AHS/ASC Structures, Structural Dynamics, and Materials Conference, AIAA Paper 91-1050-CP, Baltimore, MD, USA.

Cole, S.R., Keller, D.F., Piatak, D.J., 2000. Contributions of the NASA Langley Transonic Dynamics Tunnel to launch vehicle and spacecraft development. In: Proceedings of the AIAA Dynamics Specialists Conference, AIAA Paper 2000-1772, Atlanta, GA, USA.

Dotson, K.W., Baker, R.L., Sako, B.H., 1998a. Launch vehicle self-sustained oscillation from aeroelastic coupling part 1: theory. Journal of Spacecraft and Rockets 35, 365–373.

Dotson, K.W., Baker, R.L., Bywater, R.J., 1998b. Launch vehicle self-sustained oscillation from aeroelastic coupling part 2: analysis. Journal of Spacecraft and Rockets 35, 374–379.

Dotson, K.W., Baker, R.L., Sako, B.H., 2000. Launch vehicle buffeting with aeroelastic coupling effects. Journal of Fluids and Structures 14, 1145–1171.

Engblom, W.A., 2003. Numerical simulation of Titan IVB transonic buffet environment. Journal of Spacecraft and Rockets 40, 648–656.

Fleming, E.R., 1994. Launch vehicle loads. In: Flight-Vehicle Materials, Structures, and Dynamics—Assessment and Future Directions. New and Projected Aeronautical and Space Systems, Design Concepts, and Loads, Vol. 1, Section 2, A95-24426. ASME, New York, pp. 530–541.

Fleming, E.R., 1995. Transonic buffeting loads experience at The Aerospace Corporation. TOR-95(5530)-6, The Aerospace Corporation, Los Angeles, CA, USA.

Isakowitz, S.J., Hopkins Jr., J.P., Hopkins, J.B., 1999. International Reference Guide to Space Launch Systems, 3rd Edition. AIAA, Reston, VA, USA.

Kabe, A.M., 1998. Design and verification of launch and space vehicle structures. In: Proceedings of the 39th AIAA/ASME/ASCE/AHS/ASC Structures, Structural Dynamics, and Materials Conference, AIAA Paper 98-1718, Long Beach, CA, USA.

Lollock, J.A., 2002. The effect of swept sinusoidal excitation on the response of a single-degree-of-freedom oscillator. In: Proceedings of the 43rd AIAA/ASME/ASCE/AHS/ASC Structures, Structural Dynamics, and Materials Conference, AIAA Paper 2002-1230, Denver, CO, USA.

Oswald, J., David, F., Ruffino, F., 1999 Experimental and numerical simulation of an oscillating generic launcher. In: Proceedings of the Premier Colloque Européen sur la Technologie des Lanceurs "Vibration des Lanceurs", TP 2000-4, ONERA, Toulouse, France.

Schlichting, H., 1979. Boundary-Layer Theory, 4th Edition. McGraw-Hill, New York, NY, pp. 31–33.

Structural Dynamics Research Corp., 1998. I-DEAS Master Series 6A, Milford, OH, USA.